Journal of Applied Electrochemistry **32**: 97–104, 2002.

Electrodeposition of compositionally modulated Au/Co alloy layers

S. VALIZADEH[1]*, E.B. SVEDBERG[2] and P. LEISNER[1]
[1]*Research Institute Acreo AB, Bredgatan 34, S-602 21 Norrköping, Sweden*
[2]*Seagate Technology, Pittsburgh PA, 15203 USA*
*(*author for correspondence, e-mail: simva@acreo.se)*

Received 1 June 2000; accepted 9 October 2001

Key words: cobalt, gold, multilayers, pulse plating, single bath, Taguchi

Abstract

Au/Co multilayers were electrodeposited from a single bath based on acid citrate, cobalt sulphate and gold cyanide electrolyte. The Taguchi statistical method was used for experiment planning and optimisation. X-ray diffraction (XRD) investigations of the structure showed that the Au deposits exhibited a polycrystalline fcc ⟨1 1 1⟩ structure with an estimated grain size of ~7 nm, while the Co deposits exhibited a nano-polycrystalline fcc structure with an estimated grain size ranging between 2 and 28 nm and a strong in-plane texture. The XRD investigation of the multilayer structure also indicated an interface roughness of about 1.5 nm between the Au and Co layers.

1. Introduction

Electrodeposition of multilayers is based on two general techniques: the single-bath and the dual-bath techniques. In the single-bath technique, multilayers are grown in an electrolyte containing ions of both metals. The process can be controlled by modulating either the potential or the current density. In this method, the concentration of ions of the nobler (more electropositive) metal in the electrolyte is much lower than in the less noble metal. The properties of the electrodeposits are determined by many factors, such as the electrolyte composition, pH, temperature and agitation, the applied electrode potential and/or the current density. The dual-bath technique uses one electrolyte per metal. The substrate is activated and transferred to the first solution, plated and then rinsed and reactivated, and subsequently transferred to the second solution. The single-bath technique has the obvious advantage that the substrate always remains under the electrolyte, thus limiting the risk of contamination. However, with this technique the choice of components of the multilayers is limited. Moreover, the reduction potential of the components must be far enough apart to allow a separate electrodeposition of the components. The dual-bath technique can, with regard to this, broaden the applicability of electrodeposition as a production method for multilayers. Additionally, electrodeposition of materials has the advantage of being a low-cost process compared with sputtering, evaporation and other vacuum deposition techniques [1].

Electrodeposited Au–Co alloys, the so-called hard gold, with low cobalt content from cobalt-containing acid gold baths, are important alloys because of their high wear resistance. They have wide applications in plating electrical contacts [2–4]. Currently, in sputter-deposited Au–Co multilayers, films have been reported to possess a high perpendicular magnetic anisotropy [5–7]. Not much is known about electrodeposition of Au–Co multilayers using the single-bath technique, except for electrodeposited Au–AuCo multilayers from a commercial hard gold plating bath with high gold concentration [8]. Therefore, we attempted to electrodeposit Au–Co multilayers from a newly developed single bath with low gold concentration, which is crucial from an economic point of view. A further prospect is to improve the processing technique for fabrication of magnetic multilayered nano-wire arrays as perpendicular magnetic recording media (S. Valizadeh et al., unpublished data).

Using the single-bath technique, individual layers are plated from one solution containing two or more elements forming the multilayer deposit. A modulated composition is obtained by changing the current/potential (pulse plating) or by modulating the hydrodynamic conditions. Usually, the alloy solution contains the precious metal at low concentration and the less precious metal at much higher concentration. This means that modified alloy plating solutions or specially designed electrolytes are used [9].

In the present work, the concentration of Au was a thousand times lower than the concentration of Co. Consequently, pure Au is deposited at lower current density, whereas alloy rich in Co is deposited at a high current density, due to the mass transport limitation of the Au deposition. Galvanostatic control, rather than

potentiostatic control, was performed in order to control the layer thickness [10].

2. Experimental details

2.1. *Experimental set-up*

A rotating cylindrical electrode set-up was used, as shown schematically in Figure 1. Thick copper foils of 35 μm were used as substrates. The copper foils were cleaned for 2 s by ultrasonic rinsing. Before electroplating, the foils were electropolished in a solution containing 775 ml l^{-1} phosphoric acid and 225 ml l^{-1} propylene glycol at 350 mA cm^{-2} for 15 s. The foils were subsequently activated in 10% H_2SO_4 for 30 s. The single bath used had the following composition (in g l^{-1}): $CoSO_4 \cdot 7H_2O$ 80, $C_6H_8O_6$ 140, $KAu(CN)_2$ 0.08, KOH 120 and at pH 3.5–4. A Computer Aided Pulse Plating (CAPP) system with a rectifier from Axel Åkerman A/S was used for the plating. The anode was made of an inert platinised titanium mesh.

2.2. *Film characterisation techniques*

The film surface, morphology and chemical composition were studied by scanning electron microscopy (SEM) using a 1550 FEG instrument from Leo Co., USA and energy dispersive X-ray spectroscopy (EDS) at 20 kV. The interface topography, microstructure and layer thicknesses were investigated by X-ray diffraction (XRD) performed at high and low angles. The X-ray source, operated at 40 kV and 40 mA, was a Cu($K\alpha$ radiation) source with a Ni filter. Peak positions with accuracy in 2θ of $\pm 0.01°$ were thus obtained.

For the XRD pole figure measurements, a Philips X'Pert diffractometer with a point focus and a crossed slit (3×3 mm^2) collimator as primary optics was utilised. The diffracted beam optics was a parallel plate collimator with monochromator. Transmission electron microscopy (TEM) using a Philips EM400T microscope operated at 120 kV was employed to investigate interface characteristics and for evaluation of the Au/Co multilayer structures. Cross-sectional sample preparation for TEM analysis was performed by gluing two pieces of a sample about $0.5 \times 1 \times 2.5$ mm^3 in size with the multilayer coatings face to face in a Ti grid, which acted as a support for the sample. Prior to the ion-beam milling process, the slice was thinned to a thickness of $\sim$50 μm. Finally an electron-transparent sample was obtained using low angle Ar ion beam milling with a Bal-Tec instrument operated at 10 kV.

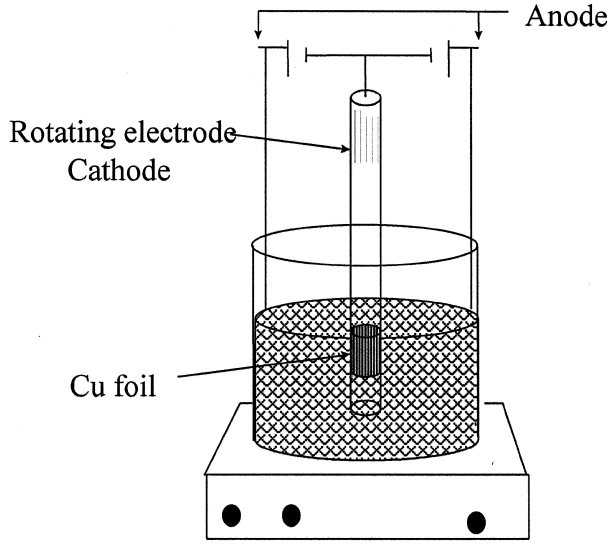

Fig. 1. The experimental set-up for electrodeposition.

2.3. *Experimental design*

The composition of the electrodeposited alloy depends on many process parameters, e.g., current density, agitation and temperature. To obtain layers of pure Au and almost pure Co from the same solution the plating parameters need to be optimised for both Au and Co, respectively. Based on introductory experiments, the overall parameter windows for depositing Au and Co layers, respectively, were established, see Tables 1 and 2. Experiments aiming at more detailed screening of the two parameter windows were designed according to Taguchi's method [11], which has proven to be very useful for the optimisation of this type of process [12].

Keeping the composition of the electrolyte constant, the intention was to identify the optimal process settings for obtaining pure deposits of Au and Co. An experimental design, a so-called L9 orthogonal array involving nine experiments, was chosen [13]. Using this design the influence of up to four parameters can be analysed, each at three different settings.

3. Results and discussions

The influence of the three parameters: current density, temperature, and agitation were analysed. The experimental plans and results are shown in Tables 3 and 4.

Table 1. Investigation of gold rich deposition

Parameters	Settings		
Current density (mA cm^{-2})	1	2	3
Temperature (°C)	25	30	40
Rotation (rpm)	400	700	1000

Table 2. Investigation of cobalt rich deposition

Parameters	Settings		
Current density (mA cm^{-2})	30	40	50
Temperature (°C)	25	30	40
Rotation (rpm)	400	700	1000

Table 3. Experimental plan and results for gold rich deposition

Exp. no.	Current density /mA cm^{-2}	Temperature/°C	Agitation /rpm	Noise check	Au /wt.%
1	1	25	400	A	95
2	1	30	700	B	97
3	1	40	1000	C	100
4	3	25	700	C	32
5	3	30	1000	A	72
6	3	40	400	B	76
7	5	25	1000	B	41
8	5	30	400	C	49
9	5	40	700	A	48

Table 4. Experimental plan and results for cobalt rich deposition

Exp. no.	Current density /mA cm^{-2}	Temperature/°C	Agitation /rpm	Noise check	Au /wt.%
1	30	25	400	A	11
2	30	30	700	B	28
3	30	40	1000	C	27
4	40	25	700	C	24
5	40	30	1000	A	24
6	40	40	400	B	7
7	50	25	1000	B	10
8	50	30	400	C	3
9	50	40	700	A	11

The fact that only three out of four possible parameters were analysed by the experimental design allowed us to get an overview of the noise in the system and interaction between the parameters. By the term 'noise' we mean all non-controlled deviations in the deposition process and the analysis. The term 'interaction' means a non-linear response when two or more parameters are changed.

3.1. *Single layer deposition*

The results, expressed by the Au content in the deposits, are shown in Tables 3 and 4 for each experiment. Based on these results, a norm is calculated for each setting of the parameters according to Taguchi's method (Figures 2 and 3). For example, the influence of the current density on the Au content was calculated from Table 3 in the following way: 1 mA cm^{-2}: (95 + 97 + 100)/3 = 97%; 3 mA cm^{-2}: (32 + 72 + 76)/3 = 60%; 5 mA cm^{-2}: (41 + 49 + 48)/3 = 46%. To check the noise in the system norm values are calculated in the same way for a fourth imaginary parameter. Since no fourth parameter was changed in reality, no variation on the calculated results should appear in the ideal situation – illustrated by horizontal dotted lines in Figures 2d and 3d. Any deviation from the horizontal lines originated from noise in the experiments and analysis or from interaction between parameters.

In Figure 2 it is seen that the most important parameter for depositing almost pure Au is low current density. The influence of the agitation on the Au content is of the same order of magnitude as the combined influence of noise and interaction on the result (Figure 2c and d). Therefore, no significant importance can be given to the agitation. The influence of the temperature is slightly more pronounced and an elevated process temperature might be preferable.

Figure 3 shows that both high current density and low agitation are significant for obtaining a low Au content in the Co deposit. Since the influence of temperature is of the same order of magnitude as the combined influence of noise and interaction, no significant importance can be given to the temperature. Considering a situation where only the deposition of Au is mass transport

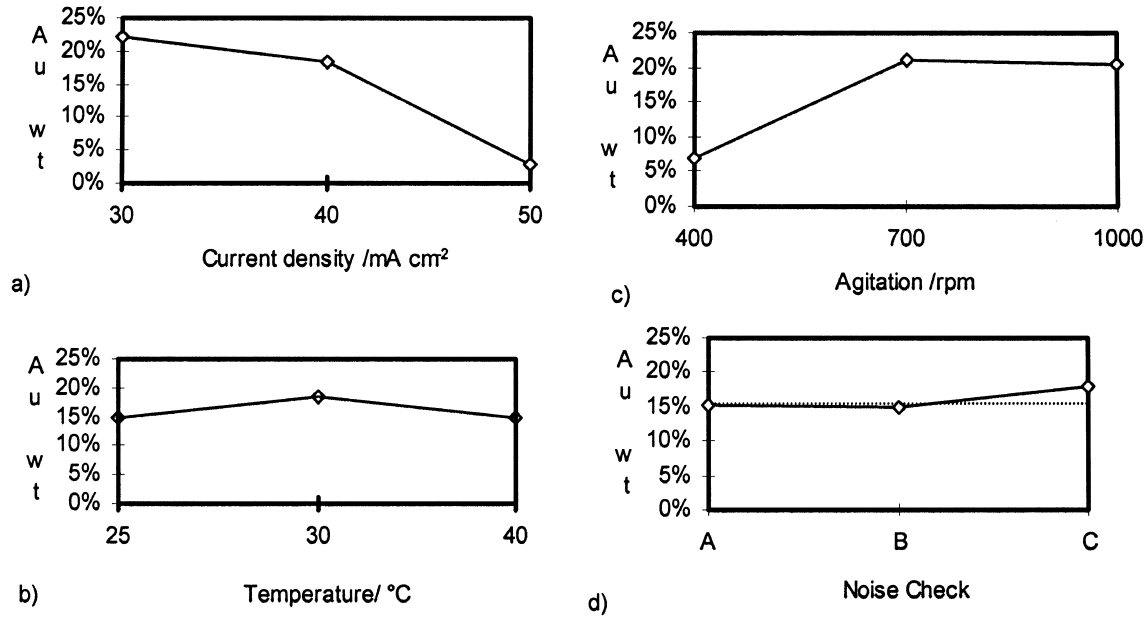

Fig. 2. Au wt.% vs variables at the low current density range. All dots in the plots are average values of three individual experiments. The dotted line in (d) represents the ideal situation without any noise in the system.

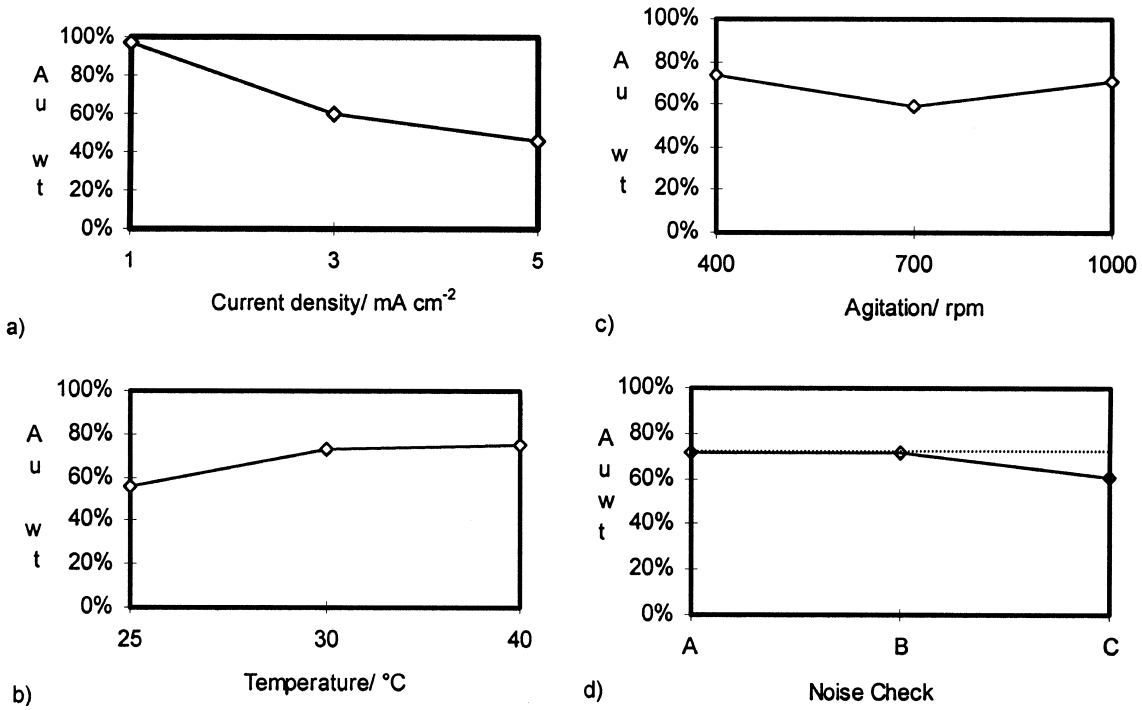

Fig. 3. Au wt.% vs variables at the high current density range. All dots in the plots are average values of three individual experiments. The dotted line in (d) represents the ideal situation without any noise in the system.

limited, the conclusions above are in accordance with the theory.

XRD analysis of pure Au deposits with a thickness of 1 μm onto a Cu substrate is shown in Figure 4. The Au deposits exhibit a polycrystalline fcc structure with an estimated grain size of $\sim$7 nm as determined by the full width at half maximum (FWHM) of the XRD peaks and the Sherrer equation [14, 15]. The larger (1 1 1) peak as compared to the (0 0 2) peak indicates a dominant $\langle 1\ 1\ 1 \rangle$ fibre texture of the gold film. Figure 5 shows an SEM image of 99 wt.% Au deposits with indistinguishable grain boundaries. However, a certain amount of nano-voids were noted (in magnified inset image) in the deposited Au layers. In other studies of Au of alloy deposits containing $\sim$0.1 wt.% cobalt, a 'void hardening' mechanism was suggested that could constitute a significant part of the increasing microhardness [2, 16–19].

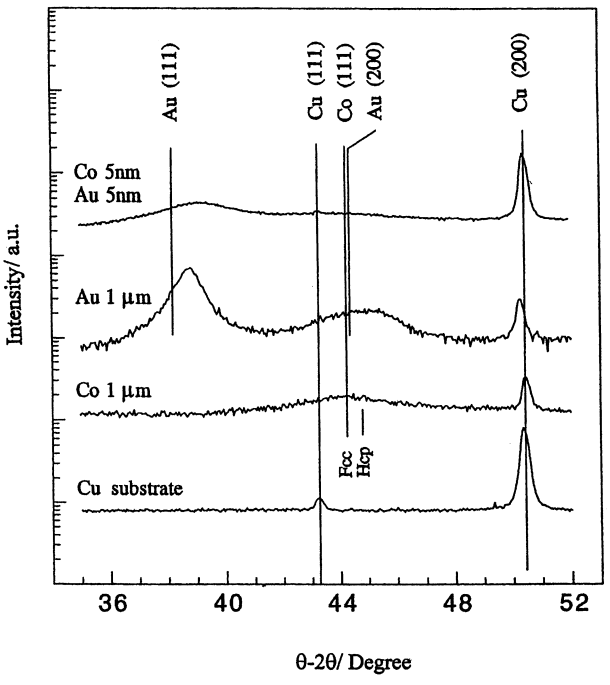

Fig. 4. $\theta - 2\theta$ XRD measurements for Co–Au multilayer as well as single Au, Co films and the substrate. The positions for bulk Au(1 1 1), Au(2 0 0) and Co(1 1 1) fcc and hcp are marked together with the Cu substrate.

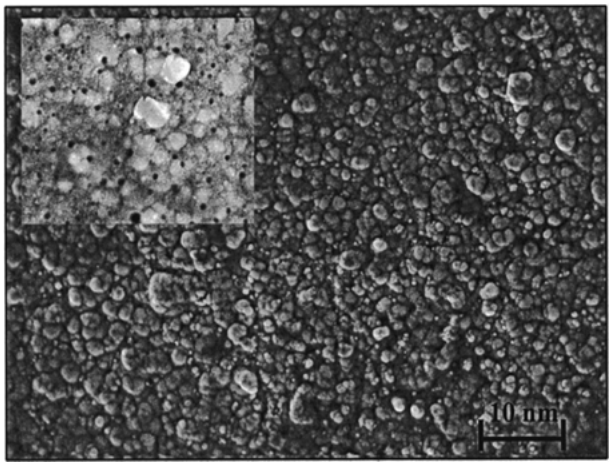

Fig. 5. SEM micrograph of 99 wt.% Au at a current density of 1 mA cm^{-2}, showing a compact deposits. The inset shows large magnification with evidence of nano-voids.

At the same time, the XRD analysis of 1 μm of almost pure Co film from Figure 4 indicated a rather weak peak around the position for a Co(1 1 1) fcc or Co(0 0 2) hcp peak. Figure 6 is an enlarged image of the Co peak, with the position of the Co(1 1 1) fcc and Co(0 0 2) hcp peaks indicated. The peak seems centred around the Co(1 1 1) fcc peak position for this almost pure Co film. However, a small concentration of Au might shift the peak to lower 2θ values, so a conclusive identification cannot be made. The Cu substrate was also measured and is shown in Figure 4. This measurement indicated a non-random texture in the polycrystalline Cu substrate with a dominant (2 0 0) texture component over the expected (1 1 1) component. Further XRD measurements revealed a mixture of Cu(2 0 0) and (2 2 0) textures in the substrates.

Complimentary to the $\theta - 2\theta$ XRD results, pole figure measurements were performed on the Co film. The pole figures of the Co and Cu were measured in Φ from 0 to 360° and Ψ from 0 to 85° in steps of 2°; a collection time of 6 s was used. The 2θ values were 44.1°, 47.57° and 50.70°, the first one corresponding to the position of a Co peak, which can be either the (0 0 2) hcp peak or the (1 1 1) cubic fcc peak. The second value corresponds to the position of the (1 0 1) peak for hexagonal Co; this peak is the most intense diffracting peak in hcp Co. Finally, 50.70° corresponds to the Cu(0 0 2) peak. As seen in Figure 7, the pole figure shows the Cu texture where the copper has a pronounced in-plane orientation, most likely due to the manufacturing process or rolling of the Cu metal sheets used in the experiments. The {0 0 2} planes probed at 50.70° introduce four intense poles, 5400 counts, at $\Psi = 33.6°$ and a weak pole in the centre, 3500 counts. The poles at 33.6° are separated 60° in Φ. In Figure 8 at $2\theta = 47.57°$ any eventual {1 0 1} hexagonal Co planes would be probed. In the centre of pole figure the intensity is at its highest but still less than 1500 counts and comparable to the background intensity in the $\theta - 2\theta$ measurements discussed previously.

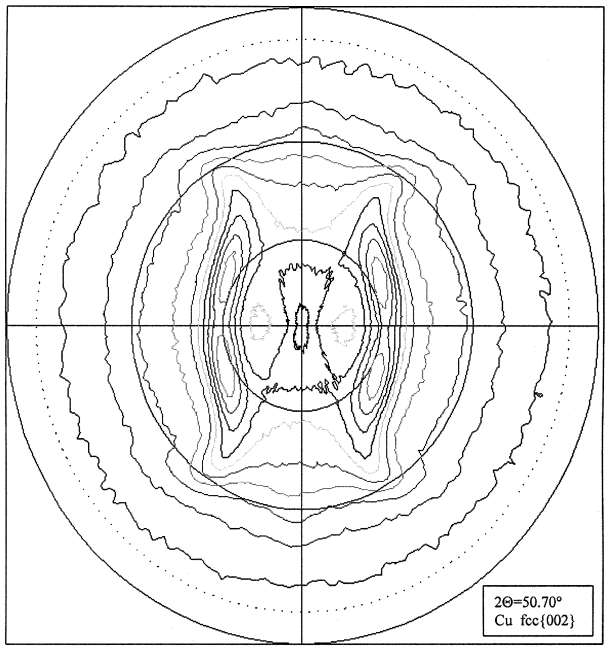

Fig. 7. Pole figure at $2\theta = 50.70°$ corresponding to the Cu(0 0 2) peak four poles are seen at $\Psi = 33.6°$ with the intensity of 5400 counts. Hence the Cu substrate has a high degree of preferred orientation.

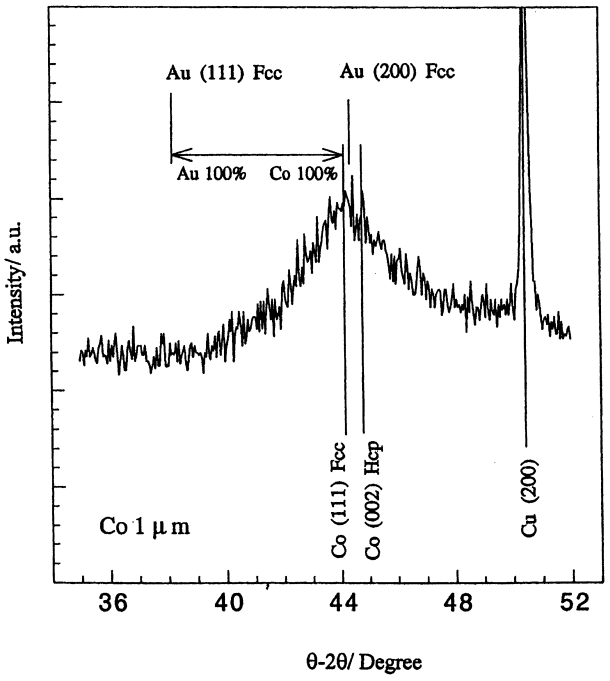

Fig. 6. $\theta - 2\theta$ XRD measurement indicating possible peak positions for Co(1 1 1) fcc and Co(0 0 2) hcp, when the Co concentration is 100% and the Au concentration is 0% for 1 μm thick film.

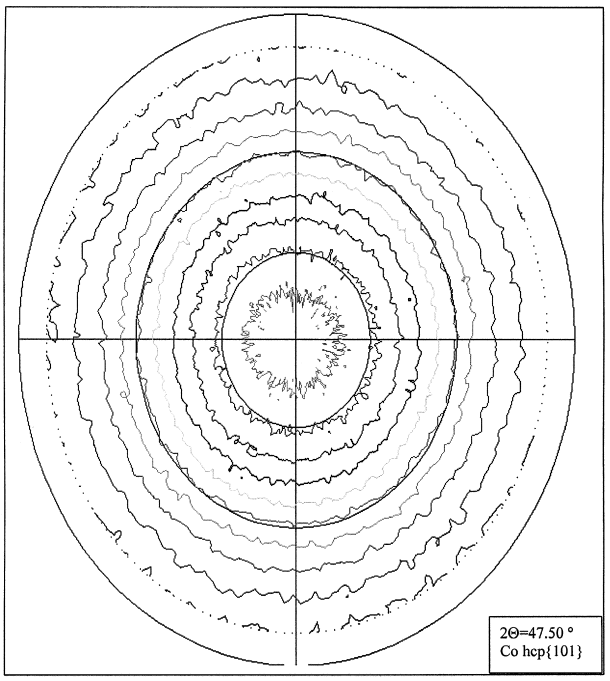

Fig. 8. Pole figure at $2\theta = 47.57°$ corresponding to Co(1 0 1) hcp peak, the highest intensity is at $\Psi = 0°$ and is less than 1500 counts and equate to the background intensity in the $\theta - 2\theta$.

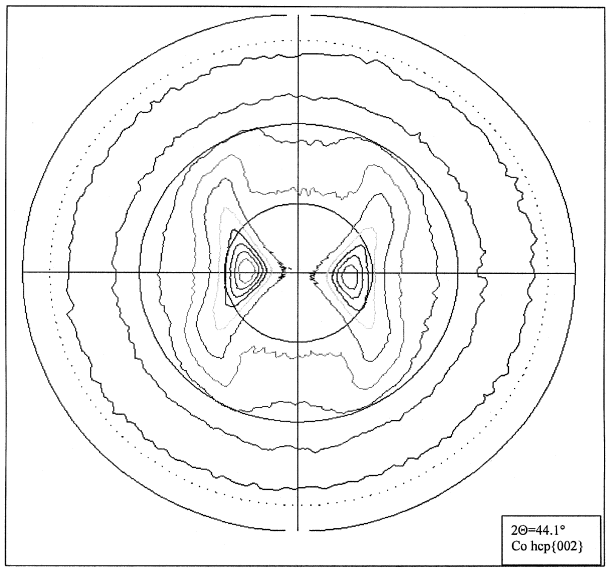

Fig. 9. Pole figure at $2\theta = 44.10°$ corresponding to the Co(0 0 2) hcp peak or (1 1 1) cubic peak two poles are seen at $\Psi = 21.3°$ with the intensity of ~12 000 counts.

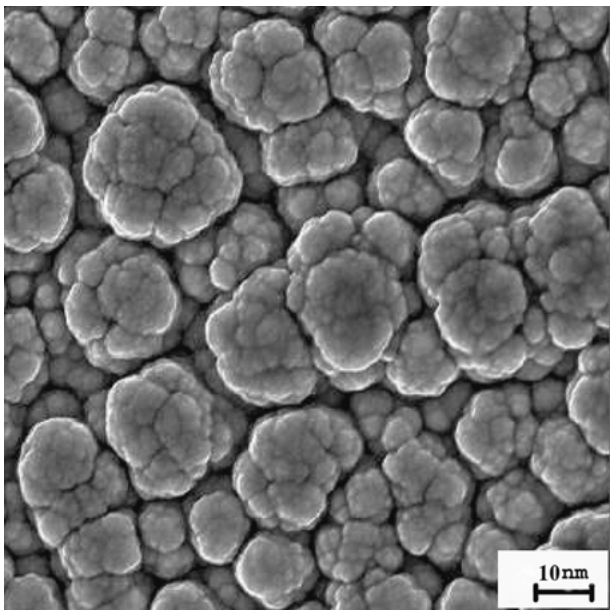

Fig. 10. SEM micrograph of 97 wt.% Co film with uniform grains produced at current density of 50 mA cm^{-2} and at 400 rpm agitation.

Further, the intensity drops rapidly with increasing Ψ value as would be expected by geometrical considerations in the measurement set-up. Hence, there is no trace of intensity from any highly diffractive {1 0 1} hcp Co planes. In Figure 9 with a 2θ value of 44.1° there are two distinct poles at $\Psi = 21.3°$ with $\Phi = 180°$ between them. These poles have an intensity of 12 000 counts. In addition, their positions are correlated to the {0 0 2} poles in the Cu substrate such that they lie symmetrically in between the Cu poles with 60° separation. In the centre of the pole figure, the intensity is just above 1500 counts, which explains why the $\theta - 2\theta$ measurements show such a weak Co peak. In light of these results, one can say that the Co is in the cubic phase and has a ⟨1 1 1⟩ texture with a high in-plane orientation where the (1 1 1) planes are tilted 21.3° from the surface plane of the Cu foil, and the texture formation in the Co film is determined in part by the texture of the Cu substrate. In addition, SEM photomicrographs of 97 wt.% Co films deposited with direct current $J =$ 50 mA cm^{-2} (Figure 10) has nodular morphology where the finest resoluble structure (grain) has an estimated size of about ~2 nm. The largest characteristic length scale was 28 nm.

3.2. *Multilayer deposition*

Based on the above results, plating conditions for deposition of Au/Co multilayers were chosen to be 25 °C and 400 rpm. In order to deposit a Co-rich layer, the deposition was initiated at 50 mA cm^{-2}, followed by open circuit condition for 12 s. Thereafter Au was deposited at 1 mA cm^{-2}. The sequence was repeated to obtain layers rich in Au and Co, respectively.

In order to investigate the quality of multilayers and the interface roughness between the Co and Au, three multilayer depositions with different layer thicknesses of 10, 100 and 150 nm were made. Table 5 summarises the parameters for the three multilayer depositions.

Figure 11 presents the multilayer coating characterisation by XRD. As seen, all the peaks in the spectra are accounted for as either Au, Co or Cu peaks. However, the only visible Co peak is the weak Co(1 1 1) peak that also overlaps slightly with the Au(0 0 2) peak. It is possible, though, to determine the Au coherence length

Table 5. Parameters for three multilayer depositions with 150, 15 and 10 cycles

Layer deposition	Current density /mA cm^{-2}	Layer thickness /nm		
Au	1	5	50	100
Co rich	50	5	50	50

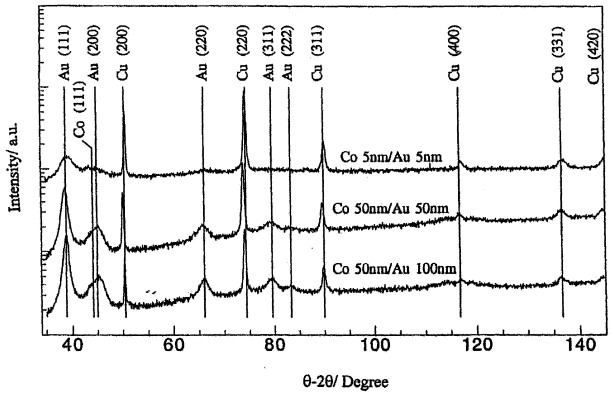

Fig. 11. XRD $\theta - 2\theta$ measurements of multilayers with wavelength 10, 100 and 150 nm. The expected positions for Co, Au and Cu peaks marked with lines.

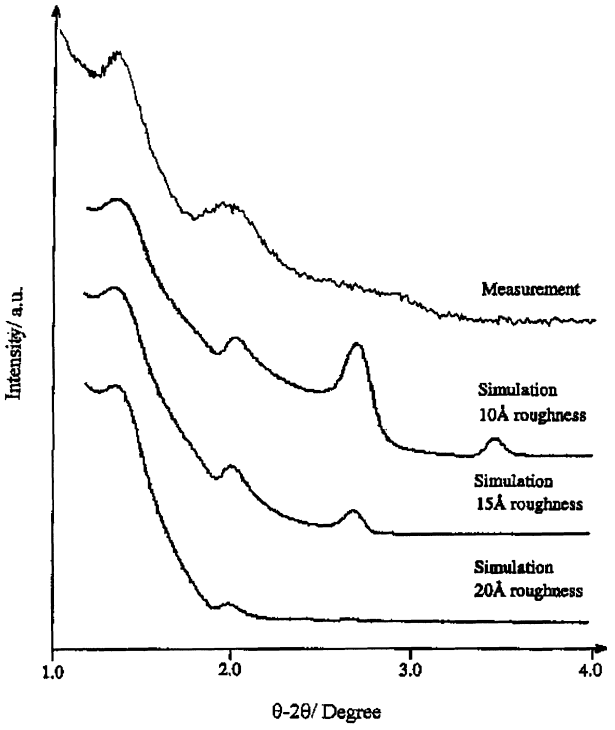

Fig. 12. Low angle XRD measurement for a short wavelength (10 nm) multilayer with characteristic peaks from a periodic chemical modulation. Also are shown the simulations of a 11 nm periodical multilayer with different interface roughness of 10, 15 and 20 Å.

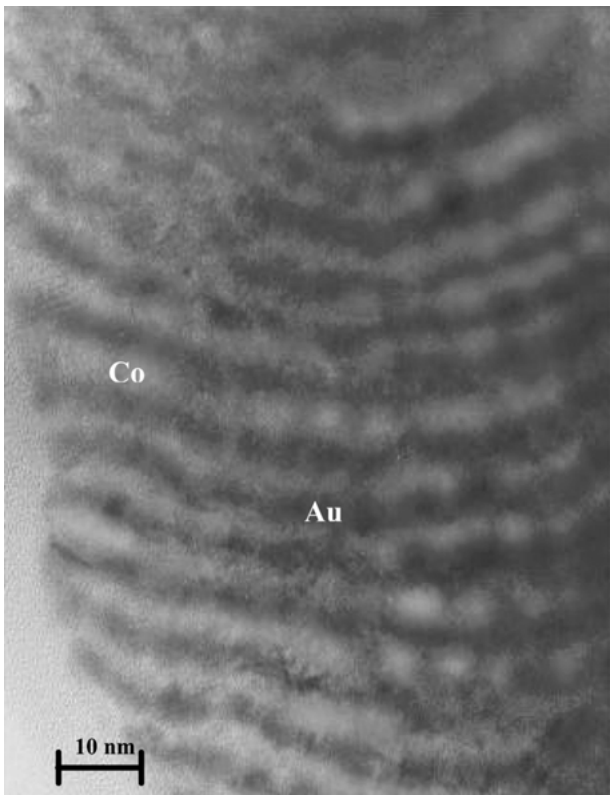

Fig. 13. XTEM image of a 5 nm Co/5 nm Au multilayer depositions. The dark layers are corresponding to Au layer and bright layers are Co layers.

or grain size out of the plane in two different films. In the Co 50 nm/Au 100 nm multilayers, the Au grain size is estimated to be ~7.3 nm, while in the multilayers with Co 50 nm/Au 50 nm, the Au grain size is estimated to ~5.8 nm. For the shortest bilayer period of 10 nm it was not possible to exactly calculate the grain size (see Figure 4), however, it is considerably smaller than for the longer bilayer period multilayers. Low angle XRD measurement for the long bilayer period, $\Lambda \geqslant 100$ nm, showed no specific XRD characteristics as would be expected for a chemical compositional modulation. Figure 12 shows a low angle XRD pattern for the sample with the expected bilayer periods of $\Lambda = 10$ nm as well as three low angle XRD simulations with bilayer period accuracy of $\Lambda = 11 \pm 1$ nm and individual layer thicknesses of 5 nm Co and 6 nm Au. The asymmetry in the different layers is detected by the fact that a perfectly symmetric superlattice, 5.0/5.0 nm, would cancel out every second peak in the low angle XRD spectra. The position of the peaks also indicates a slightly longer period, $\Lambda = 11$ nm, than the expected period of $\Lambda = 10$ nm.

Finally, the number of peaks and their amplitude can be used to estimate the interface roughness between the multilayers. Based on the simulations with layer roughness of 10, 15 and 20 Å, the simulation with 15 Å roughness fits the measured data the best. Nevertheless, no high angle XRD measurements indicate any form of superlattice structure and the diffraction pattern only shows separate broad peaks originating from the Au and Co layers, respectively. The surface morphology of the multilayers was investigated by SEM and showed a compact but rough surface with well-defined grain boundaries.

Characteristics of the multilayers were also evaluated with XTEM. Figure 13 shows a cross-sectional TEM image of a multilayer structure. Two distinguishable grey shades with relatively rough interfaces between the layers can be seen and represent the two different layers. The bright layers are the Co layers with lower atomic number than the Au. The thickness of the bilayers measured from Figure 13 contained Au/Co bilayers of 10 ± 1 nm thickness. The discrepancy between the XRD results of a bilayer thickness of 11 ± 1 nm and the TEM value of 10 ± 1 nm might be explained in light of the XRD technique as an averaging technique over a large portion of the sample and the TEM as a local probe.

4. Conclusions

A process for electrodeposition of Au–Co multilayers has been established. The Au content in the Co layers and Co content in the Au layers was minimised and found to be 3 and 0.1 wt.% respectively. The existences of multilayers were verified with both XRD and XTEM investigations. The inheritance of texture in the film from the substrate was also shown. Further, the interfacial roughness was determined to be about 1.5 nm for a coating with a bilayer thickness of about

10 nm. The XRD data showed that the electrodeposited Co rich layer films were nano-crystalline. SEM images of the deposited Co layers showed an estimated grain size of 2 nm.

It has been demonstrated that Au–Co compositionally modulated alloy layers can be made. The future aim of the work is to investigate the magnetic behaviour of deposited multilayered nano-wire arrays of these structures.

Acknowledgements

The authors are grateful to the European Commission for their financial support through the Brite EuRam program, project no. BE95-1761.

References

1. C.A. Ross, *Annu. Rev. Mater. Sci.* **24** (1994) 159.
2. E.C. Darby and S.J. Harris, *Trans. Inst. Met. Finish.* **53** (1975) 115.
3. W.H. Cleghorn, J.A. Crossley, K.J. Lodge and K.S.A. Gnanasekaran, *Trans. Inst. Met. Finish.* **50** (1972) 73.
4. L. Holt, R.J. Ellis and J. Stanyer, *Plating* **24** (1973) 9.
5. T. Takahata, S. Araki and T. Shinjo, *J. Magn. Magn. Mater.* **82** (1989) 287.
6. C. Chappert, D. Renard, P. Beauvillain and P. Bruno, *J. Magn. Magn. Mater.* **54–57** (1986) 795.
7. J.P.E. Velu, C. Dupas, D. Renard and J.P. Renard, *J. Seiden, Phys. Rev. B* **37** (1988) 668.
8. J.P. Celis, P. Cavalloti, J. Machado da Silva and A. Zielonka, *Trans. Inst. Met. Finish.* **76(5)** (1998) 163.
9. P. Leisner, C.B. Nielsen, P.T. Tag, T.C. Dörge and P. Möller, *J. Mater. Proc. Tech.* **58** (1996) 39.
10. S. Valizadeh, G. Holmbom and P. Leisner. *Surf. Coat. Technol.* **105** (1998) 213.
11. G. Taguchi, *Introduction to Quality Engineering* (Asian Productivity Organisation, Tokyo, 1998).
12. P. Leisner, D. Ulrich and P. Møller. *Plat. Surf. Finish.* **79** (1992) 62.
13. G. Taguchi and S. Konishi, *Orthogonal Arrays and Linear Graphs* (American Supplier Institute, Dearborn, MI, 1988).
14. B.D. Cullity, *Elements of X-Ray Diffraction*, (Addison-Wesley Publishing Company, 1967).
15. *Powder Diffraction file*. JCPDC International Centre for Powder Diffraction Data, Swarthmore, PA (1989).
16. C. Bechard, *J. Electrodepositors Tech. Soc.* **11** (1936) 5.
17. C.J. Stiemetz and J.J. Hern, *J. Electrochem. Soc.* **108** (1970) 64.
18. P.S. Willcox and R.J. Cady, *Plating* **60** (1973) 918.
19. Y. Okinaka and S. Nakahara, *J. Electrochem. Soc.* **123** (1976) 9.